COMMUNICATION

BaWO₂F₄: A Mixed Anion X-ray Scintillator with Excellent Photoluminescence Quantum Efficiency

Received 00th January 20xx, Accepted 00th January 20xx

DOI: 10.1039/x0xx00000x

Gyanendra B. Ayer, ^a Vladislav V. Klepov, ^a Mark D. Smith, ^a Ming Hu, ^b Zhonghua Yang, ^c Corey R. Martin, ^a Gregory Morrison, ^a and Hans-Conrad zur Loye*

A new self-activated X-ray scintillator, BaWO₂F₄, with an excellent photoluminescence quantum efficiency is reported. Hydrothermally grown single crystals, space group P2/n, exhibit a 3D framework structure containing isolated WO₂F₄ octahedra. BaWO₂F₄ exhibits green emission under UV light with a high quantum yield of 53% and scintillates when exposed to X-rays(Cu).

Scintillators, materials that emit light when struck by high energy particles or photons, are essential for medical imaging and radiation detection, including X-rays and γ -rays, and are, therefore, important materials in the field of high-energy physics, 1 nuclear power, 2 positron emission tomography (PET),³ computer tomography (CT) scanners,⁴ imaging,⁵ and more recently in homeland security for the prevention of nuclear and radiological terrorism. One prospective new class of scintillating materials are oxyhalides, in which the mixed oxide-halide environment of a scintillating cation significantly enhances its luminosity.⁶ Different classes of scintillating materials are known and include a wide variety of doped inorganic materials, 7-13 One class of materials, to which the title compound BaWO₂F₄ belongs, are the selfactivated scintillators that possess luminescent centers that are intrinsic to the structure. 14-17

Materials that are self-activated include those belonging to the scheelite ($CaWO_4$) and wolframite-type MWO_4 (M=Mg, Zn, and Cd) family, that are known to be stable and that have been used in X-ray intensifying screens and scintillators. ¹⁸ Perhaps the best known member, $CaWO_4$, displays blue emission and quantum yield of 70 % with an intense peak around 420 nm. ¹⁹ This unique optical behavior is believed to arise from the

HOMO-LUMO transition in hexavalent tungstate ions (WO₄²⁻). Due to their impact on the band gap levels, the presence of mixed anions (oxide-halide) in the structure can also play a crucial role in enhancing the intensity of luminescence and, furthermore, increase the scintillation efficiency. This reasoning is borne out in the rare earth halo-tungstates, such as La₃WO₃Cl₆, LaWO₄Cl, and GdWO₄Cl, that exhibit stronger luminescence than the corresponding halogen free tungstates. 20-22 Similarly, mixed oxide fluoride materials, such as $Cs_3RESi_4O_{10}F_2$ (RE = Y, Eu – Lu),⁶ have recently been reported to be intense scintillators, and it was shown that the presence of fluorine in the structure can increase the luminescence efficiency compared to the pure oxide compositions, such as $Eu_{9.34}(SiO_4)_6O_2$ and $NaEu_9(SiO_4)_6O_2$. Also, Toradi and Brixner investigated the compound, Ba₂WO₃F₄,²⁴ which was reported to be an excellent X-ray scintillator, in contrast to BaWO₄, which does not scintillate at all.

We explored the synthesis of mixed oxide-fluoride tungstates by employing a HF based mild hydrothermal route resulting in single crystals of the monoclinic title compound BaWO₂F₄. An orthorhombic polymorph of this compound had previously been reported as a polycrystalline powder that exhibited yellow luminescence under short wavelength UV-light. 25 The HF based mild hydrothermal route has been widely used for the crystal growth of both transition metal as well as rare earth metal fluorides and mixed oxide-fluorides.²⁶⁻³² In this method, hydrofluoric acid is used as the solvent, plays the role of a mineralizer, and acts as a fluorine source. A typical hydrothermal reaction to synthesize BaWO₂F₄ used Ba(CH₃COO)₂, WO₃, HCl and HF as the starting reagents. Heating the reagents in an autoclave to 160°C, holding at 160 e for 24 hours and slow cooling to room temperature resulted in a mixed phase product consisting of colorless rod crystals of BaWO₂F₄ in an approximately 30 % yield along with BaClF powder as an impurity. The impurity could be removed by sonication in acetone followed by decanting. As this initial HF based mild hydrothermal route did not result in a phase pure product and only in low yield, we developed a two-step process to generate larger quantities of pure BaWO₂F₄.

Electronic Supplementary Information (ESI) available: [details of any supplementary information available should be included here]. See DOI: 10.1039/x0xx00000x

^{a.} Department of Chemistry and Biochemistry, University of South Carolina, Columbia, SC, United States. E-mail: zurloye@mailbox.sc.edu

b. Department of Mechanical Engineering, University of South Carolina, Columbia,
SC, United States

c. Department of Architectural and Civil Engineering, Shenyang University of Technology, Shenyang, Liaoning, China

COMMUNICATION DALTON TRANSACTIONS

Specifically, creating freshly precipitated BaWO₄ and reacting it with HF under hydrothermal conditions results in the formation of phase pure BaWO₂F₄. It is important to note that the transformation of the oxide to the oxyfluoride involves the conversion of the WO₄²⁻ tetrahedra in BaWO₄ into the WO₂F₄²⁻ octahedra in BaWO₂F₄. This change in composition and coordination environment around the tungsten leads to bright luminescence and scintillation that is not observed in BaWO₄. $BaWO_2F_4$ crystallizes in the monoclinic space group P2/n and its asymmetric unit contains two Ba, two W, four O and eight F sites. The structure is a framework that consists of WO₂F₄ octahedra isolated from each other by Ba cations. The O atoms are cis in the WO₂F₄ octahedron, similar to those found in the related Na₂WO₂F₄ composition.³³ The tungsten in BaWO₂F₄ is located in a WO_2F_4 coordination environment with $C_{2\nu}$ symmetry in the shape of an octahedron (Figure 1a). The two equatorial W-O bonds of both the tungsten sites are slightly shorter, 1.703(5)-1.743(5) Å, than the two axial W-F bonds, 1.885(4)-1.953(4) Å and the two equatorial W-F bonds, 2.042(4)-2.083(4) Å. The O-W-O angles of the octahedron fall within a narrow range of 103.5(3)-104.1(3)° and the F-W-F angles lie within the range of 74.38(16)-166.6(2)°, forming a cis-[WO₂F₄]²⁻ distortion that contributes to the luminescence of the material vide infra. The distorted tungsten octahedra are separated from each other and are arranged along the aaxis (Figure 1b). The large voids in the structure are occupied by the barium cations, which connect the isolated tungsten octahedral units into a three dimensional framework structure (Figure 1c).

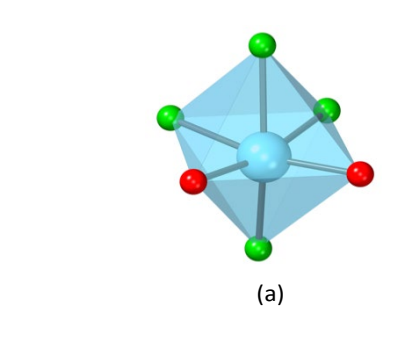
The excitation and emission spectra of $BaWO_2F_4$ measured at 300 K are shown in Figure 2. When excited at 286 nm, the emission spectrum displays a broad peak centered at ~520 nm, which lies in the green region of the visual spectrum 492–575 nm. Exposing ground crystals to X-rays results in intense green scintillation as shown in Figure 3.

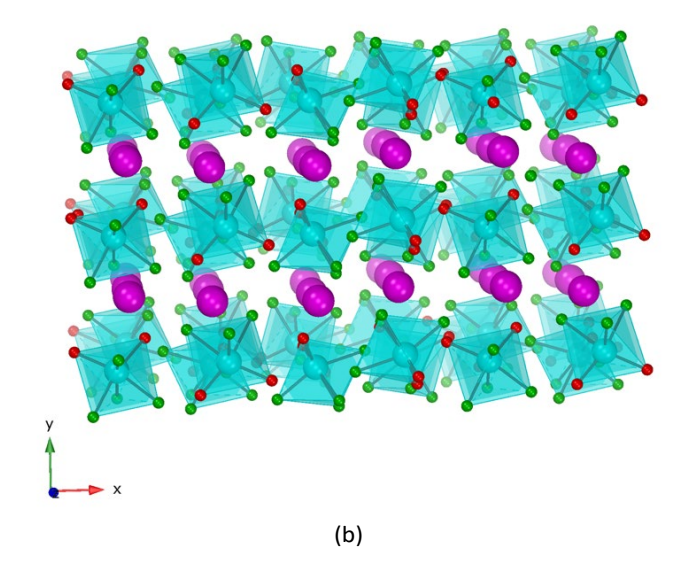
The key reason for the intense luminescence and scintillation of this compound, relative to $BaWO_4$, is due to the structural and compositional difference of the tungsten luminescent center, a distorted WO_2F_4 octahedron in $BaWO_2F_4$ and regular WO_4 tetrahedron in $BaWO_4$. The intrinsic luminescence of scheelite-type tungstates, MWO_4 (M = Ca, Ba, and Pb), is usually attributed to excitons, located on the WO_4 tetrahedra, that can migrate through the crystal lattice.³⁴

To better understand the difference in the photoluminescence in $BaWO_2F_4$ and $BaWO_4$ and in particular the role the fluorine ion plays, DFT calculations were performed, since, this method has been widely employed to better understand the structure-property relationships for various optical materials. To one important result of the DFT calculations (vide infra) is the fact that the fluorine strongly interacts with the tungsten via orbital overlap and hybridization between the W5d level and the F2p level in the -5 – 0 eV energy range at the top of the valence band, resulting in a distorted WO_2F_4 octahedron. Hence, fluorine plays a key structural role that influences the luminescence and scintillating behavior of $BaWO_2F_4$.

The photoelectric properties of materials are mainly characterized by the dielectric function, the refractive

coefficient, the absorption coefficient, and these optical constants are determined by the band structure, carrier concentration, and mobility near the Fermi surface. Therefore, we calculate the band structure of BaWO₄ and found that it is a direct bandgap material with the valence-band maxima and conduction-band minima both located at the Γ point (Figure 4a). The calculated value of the bandgap energy (E_g) for BaWO₄ of 4.5862 eV is in excellent agreement with a previous study.³⁸ Compared with BaWO₄, the E_g of BaWO₂F₄ is reduced to 1.2962 eV, due to the presence of isolated bands that result from the splitting of the





Dalton Transactions COMMUNICATION

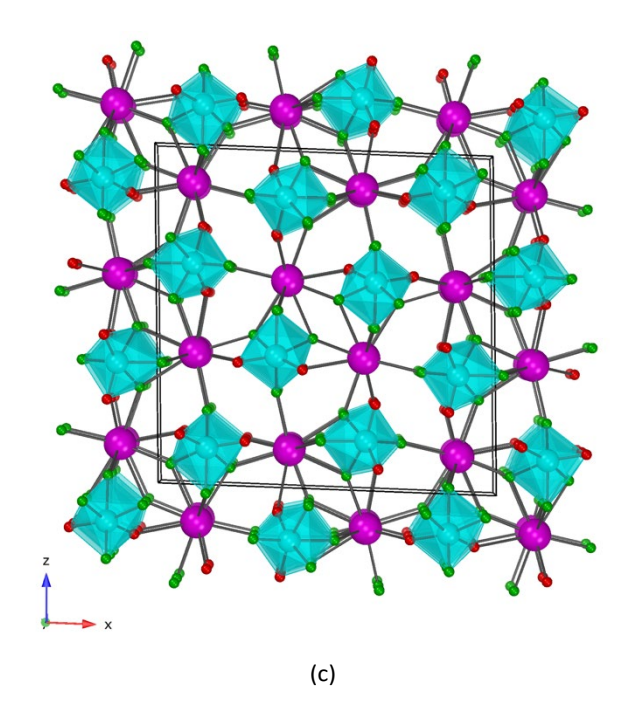


Figure 1. (a) Illustration of a WO_2F_4 octahedron. (b and c) A view of the BaWO₂F₄ structure along the *c* and *b* axes, respectively. The tungsten, barium, oxygen, and fluorine atoms are shown in light blue, pink, red, and green, respectively.

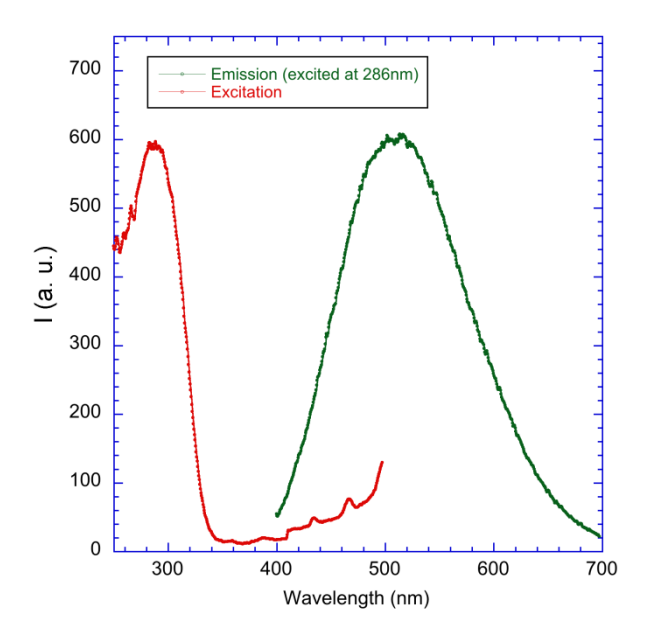


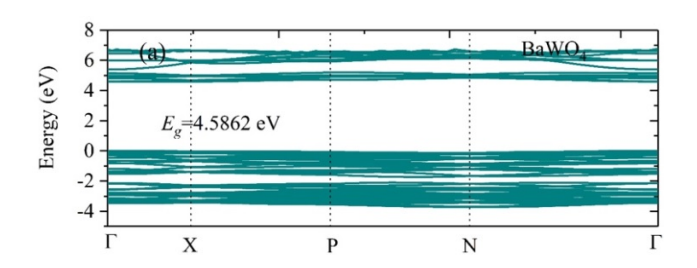
Figure 2. Luminescence spectra for $BaWO_2F_4$





Figure 3. (left) Optical image of ground crystals of BaWO₂F₄ in the absence of X-rays and (right) optical image of scintillating ground crystals when exposed to X-rays.

conduction band. This split energy band is mainly W 5s in nature and significantly reduces the bandgap (Figure 5b). Figure 5 shows the total density of states (TDOS) and partial density of states (PDOS) of BaWO₄ and BaWO₂F₄. As can be seen in Figure 5a, there exists a large gap between the valence and conduction bands, which is consistent with the band structure of BaWO₄ in Figure 4a. For the TDOS and PDOS of BaWO₂F₄ (Figure 5b), the W 5d level forms the lower conduction band, since W is more electronegative than Ba and the upper conduction bands are composed by the more electropositive Ba 6d level. On the other hand, the valence bands are dominated by filled 2p levels belonging to the mixed anion (oxygen/fluorine) sites. It is worth highlighting that in comparison with BaWO₄, a new TDOS peak of BaWO₂F₄ appears at the bottom of the conduction band, the result of the band splitting mentioned above. This new peak is attributed to the W 5s levels, which is not observed in BaWO₄, and is essential for the observed luminescence and scintillation.



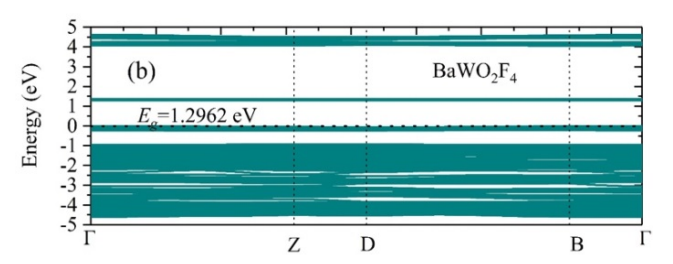


Figure 4. Band structure of (a) BaWO₄ and (b) BaWO₂F₄ with bandgap labeled.

COMMUNICATION DALTON TRANSACTIONS

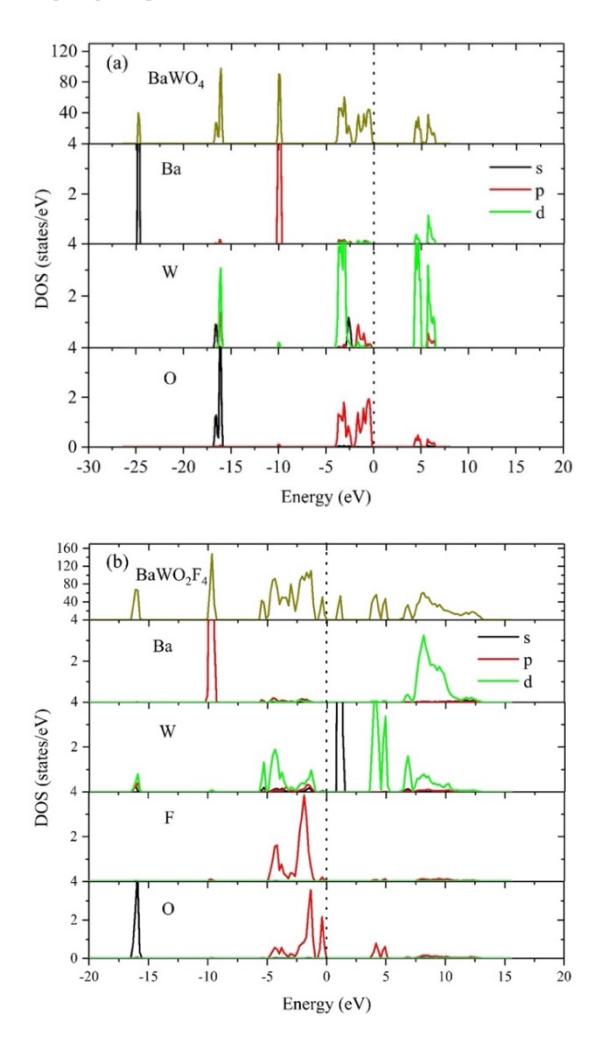


Figure 5. Total density of states and partial density of states of (a) $BaWO_4$ and (b) $BaWO_2F_4$.

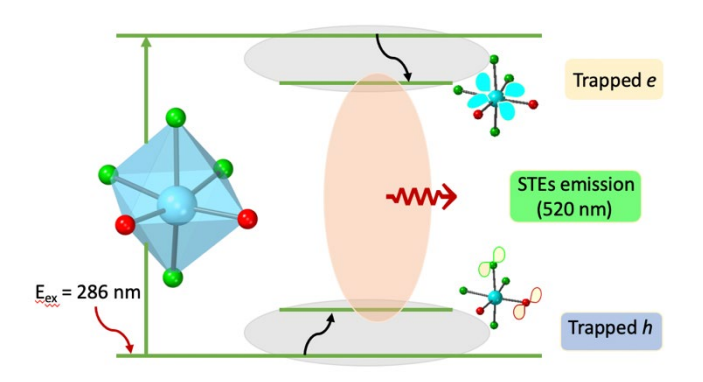


Figure **6**. A simplified illustration of the hypothetical process of photoluminescence in $BaWO_2F_4$.

The observed conduction band splitting is not unusual and, in fact, exists in other compounds where it is known to impact luminescent behavior.³⁹ In addition, the large W-W bond distance (6.520 Å), shown in Figure S3b, reduces the orbital overlap resulting in narrow bands that can stabilize self-trapped excitons (STEs) and promote strong exciton emission at room temperature. By comparison, the luminescence

mechanism in the inorganic perovskite halides is governed by self-trapped excitons (STEs), which are strongly localized at the isolated metal halide octahedra. In such compounds, the strong spatial localization and the absence of electron trapping processes favors radiative recombination, resulting in the highly localized Frenkel-like excitons rather than Wannier-Mott type excitons. Furthermore, in tungsten based mixed anion compound, $K_3WO_3F_3$, the distorted WO_3F_3 octahedron plays an important role in trapping localized charge carriers, which forms many low energy excitonic bands or self-trapped excitons (STEs). Hence, one can postulate that the visible emission in $BaWO_2F_4$ is due to the formation of self-trapped excitons (STEs) at the excitonic or polaronic levels within the forbidden gap, that is responsible for the luminescence and scintillation of the compound (Figure 6).

The thermal behavior of BaWO $_2$ F $_4$ was studied using thermogravimetric analysis (TGA) up to 1200 °C under an oxygen gas flow (Figure S4). The TGA data indicate that a slight weight loss, likely due to absorbed moisture, takes place at low temperatures. Above 400 °C the sample undergoes a larger weight loss due to thermal decomposition. Heating the material in air above 400 °C resulted in the formation of BaWO $_4$, Figure S5, which indicates that BaWO $_2$ F $_4$ oxidizes on heating in air with the release of four molecules of hydrofluoric acid.

In summary, high quality single crystals of $BaWO_2F_4$ were synthesized using an HF based mild hydrothermal synthesis. The compound crystallizes in the monoclinic P2/n space group and consists of isolated $WO_2F_4^{2-}$ distorted octahedra separated by barium cations. The compound emits intense green light under UV light and, furthermore, emits green light under X-ray irradiation. The observed luminescence in this compound is attributed to highly localized self-trapped excitons (STEs) situated at the isolated metal octahedra.

Conflicts of interest

There are no conflicts to declare.

Acknowledgements

Financial support for this work was provided by the National Science Foundation under award DMR-1806279 and is gratefully acknowledged.

CCDC #2007855 contain the supplementary crystallographic data for this paper. These data can be obtained free of charge via www.ccdc.cam.ac.uk/data_request/cif, or by emailing data_request@ccdc.cam.ac.uk, or by contacting The Cambridge Crystallographic Data Centre, 12 Union Road, Cambridge CB2 1EZ, UK; fax: +44 1223 336033.

Notes and references

Dalton Transactions COMMUNICATION

- [1] Nikl, M.; Yoshikawa, A. Recent R&D Trends in Inorganic Single-Crystal Scintillator Materials for Radiation Detection. *Adv. Opt. Mater.* **2015**, *3*, 463–481.
- [2] Martin, T.; Koch, A.; Nikl, M. Scintillator materials for x-ray detectors and beam monitors. *MRS Bull.* **2017**, *42*, 451–457.
- [3] Eriksson, L.; Melcher, C. L.; Eriksson, M.; Rothfuss, H.; Grazioso, R.; Aykac, M. Design Considerations of Phoswich Detectors for High Resolution Positron Emission Tomography. *IEEE Trans. on Nucl. Sci.* **2009**, *56*, 182–188.
- [4] Touš, J.; Blažek, K.; Pína, L.; Sopko, B. High-resolution imaging of biological and other objects with an X-ray digital camera. *Appl. Radiat. Isot.* **2010**, *68*, 651–653.
- [5] Ronda, C.; Wieczorek, H.; Khanin, V.; Rodnyi, P. Review-Scintillators for Medical Imaging: A Tutorial Overview. *ECS J. Solid State Sci. Technol.* **2016**, 5, R3121.
- [6] Morrison, G.; Latshaw, A. M.; Spagnuolo, N. R.; zur Loye, H.-C. Observation of Intense X-ray Scintillation in a Family of Mixed Anion Silicates, $Cs_3RESi_4O_{10}F$ (RE = Y, Eu-Lu), Obtained via an Enhanced Flux Crystal Growth Technique. *J. Am. Chem. Soc.* **2017**, *139*, 14743–14748.
- [7]West, H. I.; Meyerhof, W. E.; Hofstadter, R. Detection of X-rays by means of NaI(TI) scintillation counters. *Phys. Rev.* **1951**, *81*,141–142.
- [8] Nagarkar, V. V.; Gupta, T. K.; Miller, S. R.; Klugerman, Y.; Squillante, M. R.; Entine, G. Structured CsI(TI) scintillators for X-ray imaging applications. *IEEE Trans. Nucl. Sci.* **1998**, *45*, 492–496.
- [9] van Loef, E. V. D.; Dorenbos, P.; van Eijk, C. W. E.; Krämer, K.; Güdel, H. U. High-energy-resolution scintillator: Ce³⁺ activated LaBr₃. *Appl. Phys. Lett.* **2001**, *79*, 1573–75.
- [10] Alekhin, M. S.; de Haas, J. T. M.; Kramer, K. W.; Dorenbos, P. Scintillation Properties of and Self Absorption in Srl₂:Eu²⁺. *IEEE Trans. Nucl. Sci.* **2011**, *58*, 2519–2527.
- [11] Stand, L.; Zhuravleva, M.; Chakoumakos, B.; Johnson, J.; Loyd, M.; Wu, Y.; Koschan, M.; Melcher, C. L. Crystal Growth and Scintillation Properties of Eu²⁺ doped Cs₄Cal₆ and Cs₄Srl₆. *J. Cryst. Growth.* **2018**, *486*, 162–168.
- [12] Zhuravleva, M.; Blalock, B.; Yang, K.; Koschan, M.; Melcher, C. L. New single crystal scintillators: CsCaCl₃:Eu and CsCal₃:Eu. *J. Cryst. Growth.* **2012**, *352*, 115–119.
- [13] Zhuravleva, M.; Friedrich, S.; Melcher, C. L. The europium oxidation state in CsSrl₃:Eu scintillators measured by X-ray absorption spectroscopy. *Opt. Mater.* **2014**, *36*, 670–674.
- [14] Yahaba, N.; Koshimizu, M.; Sun, Y.; Yanagida, T.; Fujimoto, Y.; Haruki, R.; Nishikido, F.; Kishimoto, S.; Asai, K. X-ray detection capability of a Cs₂ZnCl₄ single-crystal scintillator. *Appl. Phys. Express* **2014**, *7*, 062602.
- [15] Shimizu, M.; Koshimizu, M.; Fujimoto, Y.; Yanagida, T.; Ono, S.; Asai, K. Luminescence and scintillation properties of Cs₃BiCl₆ crystals. *Opt. Mater.* **2016**, *61*, 115–118.
- [16] Saeki, K.; Wakai, Y.; Fujimoto, Y.; Koshimizu, M.; Yanagida, T.; Nakauchi, D.; Asai, K. Luminescence and scintillation properties of Rb₂HfCl₆ crystals. *Jpn. J. Appl. Phys.* **2016**, *55*, 110311.
- [17] Klintenberg, M. K.; Weber, M. J.; Derenzo, D. E. Luminescence and scintillation of Pbl_2 and Hgl_2 . *J. Lumin.* **2003**, 102-103, 287-290.

- [18] Feldmann, C.; Jüstel, T.; Ronda, C. R.; Schmidt, P. J. Inorganic Luminescent Materials: 100 Years of Research and Application. *Adv. Funct. Mater.* **2003**, *13*, 511–516.
- [19] Mai, M.; Feldmann, C. Microemulsion-based synthesis and luminescence of nanoparticulate CaWO₄, ZnWO₄, CaWO₄:Tb, and CaWO₄:Eu. *J. Mater. Sci.* **2012**, *47*, 1427–1435.
- [20] Brixner, L. H.; Chen, H. Y.; Foris, C. M. Structure and luminescence of the orthorhombic LnWO₄Cl-type rare earth halo tungstates. *J. Solid State Chem.***1982**, *45*, 80–87.
- [21] Brixner, L. H.; Chen, H. Y.; Foris, C. M. Structure and luminescence of some rare earth halotungstates of the type Ln₃WO₆Cl₃. *J. Solid State Chem.***1982**, *44*, 99–107.
- [22] Blasse, G.; Dirksen, G. J.; Brixner, L. H. Luminescence properties of uranium-activated lanthanum halotungstate (La₃WO₆Cl₃ <u>U</u>). *J. Solid State Chem.* **1982**, *44*, 162–68.
- [23] Latshaw, A. M.; Hughey, K. D.; Smith, M. D.; Yeon, J.; zur Loye, H.-C. Photoluminescent and magnetic properties of lanthanide containing apatites: $Na_x Ln_{10-x}(SiO_4)_6O_{2-y}F_y$,
- $Ca_xLn_{10-x}(SiO_4)_6O_{2-y}F_y$ (Ln = Eu, Gd, and Sm), $Gd_{9.34}(SiO_4)_6O_2$, and $K_{1.32}Pr_{8.68}(SiO_4)_6O_{1.36}F_{0.64}$. *Inorg. Chem.* **2015**, *54*, 876–884.
- [24] Torardi, C. C.; Brixner, L. H. Structure and luminescence of Ba₂WO₃F₄. *MRS Bull.* **1985**, *20*, 137–145.
- [25] Srivastava, A. M.; Ackerman, J. F. Synthesis and luminescence of dioxo W^{6+} (d^0) complex: BaWO₂F₄. *Mater. Res. Bull.* **1999**, *34*, 1397–1402.
- [26] Norquist, A. J.; Heier, K. R.; Stern, C. L.; Poeppelmeier, K. R. Composition Space Diagrams for Mixed Transition Metal Oxide Fluorides. *Inorg. Chem.* **1998**, *37*, 6495–6501.
- [27] Ayer, G. B.; Klepov, V. V.; Smith, M. D.; zur Loye, H.-C. Mild Hydrothermal Synthesis of the Complex Hafnium-Containing Fluorides $Cs_2[M(H_2O)_6][Hf_2F_{12}]$ (M = Ni, Co, Zn), CuHfF₆(H₂O)₄, and $Cs_2Hf_3Mn_3F_{20}$ Based on HfF₇ and HfF₆ Coordination Polyhedra. *Inorg. Chem.* **2019**, *58*, 13049–13057.
- [28] Klepov, V. V.; Pace, K. A.; Calder, S.; Felder, J. B.; zur Loye, H.-C. 3d-Metal Induced Magnetic Ordering on U(IV) Atoms as a Route toward U(IV) Magnetic Materials. *J. Am. Chem. Soc.* **2019**, *141*, 3838–3842.
- [29] Talley, C. E.; Bean, A. C.; Albrecht-Schmitt, T. E. Hydrothermal syntheses of layered uranium oxyfluorides: illustrations of dimensional reduction. *Inorg. Chem.* **2000**, *39*, 5174–5175.
- [30] Felder, J. B.; Smith, M. D.; zur Loye, H.-C. Utilizing an In Situ Reduction in the Synthesis of BaMoOF₅. *J. Chem. Crystallogr.* **2019**, *49*, 52–57.
- [31] Ayer, G. B.; Klepov, V. V.; Pace, K. A.; zur Loye, H.-C. Quaternary Cerium(IV) Containing Fluorides Exhibiting Ce_3F_{16} Sheets and Ce_6F_{30} Frameworks. *Dalton Trans.* **2020**, *49*, 5898–5905.
- [32] Allen, S.; Barlow, S.; Halasyamani, P. S.; Mosselmans, J. F. W.; O'Hare, D.; Walker, S. M.; Walton, R. I. Hydrothermal Synthesis of $(C_6N_2H_{14})_2(U^{Vl}_2U^{lv}O_4F_{12})$, a Mixed-Valent One-Dimensional Uranium Oxyfluoride. *Inorg. Chem.* **2000**, *39*, 3791–3798.
- [33] Chaminade, J. P.; Moutou, J. M.; Villeneuve, G.; Couzi, M.; Pouchard, M.; Hagenmuller, P. Oxygen-flour order in oxyfluorides $Na_2WO_2F_4$, LiW_3O_9F , and $NaMoO_3F$. *J. Solid State Chem.* **1986**, *65*, 27–39.

COMMUNICATION DALTON TRANSACTIONS

- [34] Kolobanov, V. N.; Kamenskikh, I. A.; Mikhailin, V. V.; Shpinkov, I. N.; Spassky, D. A.; Zadneprovsky, B. I.; Potkin, L. I.; Zimmerer, G. Optical and luminescent properties of anisotropic tungstate crystals. *Nucl. Instrum. Methods Phys. Res A* **2002**, *486*, 496–503.
- [35] Li, L.; Wang, Y.; Lei, B.-H.; Han, S.; Yang, Z.; Poeppelmeier, K. R.; Pan, S. A New Deep-Ultraviolet Transparent Orthophosphate LiCs₂PO₄ with Large Second Harmonic Generation Response. *J. Am. Chem. Soc.* **2016**, *138*, 9101-9104. [36] Abudoureheman, M.; Han, S.; Lei, B.-H.; Yang, Z.; Long, X.; Pan, S. KPb₂(PO₃)₅: a novel nonlinear optical lead polyphosphate with a short deep-UV cutoff edge. *J. Mater. Chem. C* **2016**, *4*, 10630-10637.
- [37] Li, L.; Wang, Y.; Lei, B.-H.; Han, S.; Yang, Z.; Li, H.; Pan, S. LiRb₂PO₄: a new deep-ultraviolet nonlinear optical phosphate with a large SHG response. *J. Mater. Chem. C* **2017**, *5*, 269-274. [38] Carvalho, I. P.; Lima, A. F.; Lalic, M. V. Theoretical study of electronic and optical properties of the scheelite MWO₄ (M = Ca, Sr or Ba) compounds by applying the modified Becke-Johnson exchange-correlation potential. *Opt. Mater.* **2019**, *92*, 187–194.
- [39] Shi, H.; Du, M.-H. Discrete Electronic Bands in Semiconductors and Insulators: Potential High-Light-Yield Scintillators. *Phys. Rev. Appl.* **2015**, *3*, 054005.
- [40] Benin, B. M.; Dirin, D. N.; Morad, V.; Wörle, M.; Yakunin, S.; Rainò, G.; Nazarenko, O.; Fischer, M.; Infante, I.; Kovalenko, M. V. Highly Emissive Self-Trapped Excitons in Fully Inorganic Zero-Dimensional Tin Halides. *Angew. Chem. Int. Ed. Engl.* **2018**, *57*, 11329–11333.
- [41] Wu, Y.; Han, D.; Chakoumakos, B. C.; Shi, H.; Chen, S.; Du, M.-H.; Greeley, I.; Loyd, M.; Rutstrom, D. J.; Stand, L.; Koschan, M.; Melcher, C. L. Zero-dimensional Cs_4EuX_6 (X = Br, I) allinorganic perovskite single crystals for gamma-ray spectroscopy. *J. Mater. Chem. C* **2018**, *6*, 6647–6655.
- [42] Omelkov, S. I.; Spassky, D. A.; Pustovarov, V. A.; Kozlov, A. V.; Isaenko, L. I. Time-resolved luminescence spectroscopy of structurally disordered K₃WO₃F₃ crystals. *Opt. Mater.* **2016**, *58*, 285–289.